Independent-component analysis of skin color image

Norimichi Tsumura, Hideaki Haneishi, and Yoichi Miyake

Department of Information and Image Sciences, Chiba University 1-33, Yayoi-cho, Inage-ku, Chiba 263-8522, Japan

Received January 13, 1999; accepted April 28, 1999

The spatial distributions of melanin and hemoglobin in human skin are separated by independent-component analysis of a skin color image. The analysis is based on the skin color model with three assumptions: (1) Spatial variation of color in the skin is caused by two pigments, melanin and hemoglobin; (2) the quantities of the two pigments are mutually independent spatially; and (3) linearity holds among the quantities and the observed color signals in the optical density domain. The results of the separation agree well with physiological knowledge. The separated components are synthesized to simulate the various facial color images by changing the quantities of the two separated pigments. © 1999 Optical Society of America
[S0740-3232(99)00609-2]

OCIS codes: 100.2960, 330.1690.

1. INTRODUCTION

Skin color reproduction may be considered the most important problem in the color reproduction of color film and color television systems.[1] With the recent progress in various imaging systems[2–5] such as multimedia, computer graphic, and telemedicine systems, skin color becomes increasingly important for communication, image reproduction on hard copy and soft copy, medical diagnosis, cosmetic development, and so on.

Human skin is a turbid medium with multilayered structure.[6,7] Various pigments such as melanin and hemoglobin are contained in the medium. Slight changes in structure and pigment construction produce rich skin color variation.[8] Therefore it is necessary to analyze skin color on the basis of structure and pigment construction in reproducing and discerning various skin colors.

In this paper the spatial distributions of melanin and hemoglobin in skin are separated by independent-component analysis (ICA) of a skin color image. ICA is a technique that extracts the original signals from mixtures of many independent sources without *a priori* information on the sources and the process of the mixture. ICA has been applied to various problems such as array processing, communication, medical signal processing, and speech processing.[9] In the field of color image processing, Inoue *et al.*[10] proposed a technique to separate each pigment from compound color images. Their research is reviewed in Section 2 in this paper. However, they could not obtain any practical results, since they assumed linearity among the quantities of pigments and observed color signals in the intensity domain, and in the intensity domain this linearity generally will not hold in practical applications. We improve on their technique by processing color signals in the density domain and applying the technique to analyze the skin color image. Furthermore, we apply the result of the analysis to the separation and synthesis of a facial color image.

In Section 2 we review the independent-component analysis proposed in Ref. 10 for application to color image separation. In Section 3 skin color is modeled on the basis of the two pigments melanin and hemoglobin in the optical density domain. The results of the independent-component analysis for skin color images are shown in Section 4. In Section 5, separated and synthesized facial color images are shown.

2. INDEPENDENT-COMPONENT ANALYSIS

ICA is a technique that extracts the original signals from mixtures of many independent sources without *a priori* information on the sources and the process of the mixture. To apply ICA to color image separation, Inoue *et al.*[10] considered that the quantities of the pigments that construct the color are the original signals from independent sources, the observed color signals are mixtures, and the pure color signals of the pigments indicate the mixing process of the quantities.[10] In this section we describe this technique as developed in Ref. 10.

Simplifying the description, we assume that the medium is constructed by two pigments and that it is captured by an imaging system with two color channels. This simplification does not prevent generalization of the problem except when the number of pigments is larger than the number of channels. This situation is discussed below.

Let $x_{l,m}(1)$ and $x_{l,m}(2)$ denote the quantities of the two pigments on the coordinates (l, m) in the digital color image and $\mathbf{a}(1)$ and $\mathbf{a}(2)$denote pure color vectors of the two pigments per unit quantity, respectively. Inoue *et al.*[10] assumed that $\mathbf{a}(1)$and $\mathbf{a}(2)$ are different from each other. They also assumed that the compound color vector $\mathbf{e}_{l,m}$ on the image coordinates (l, m) can be calculated by the linear combination of pure color vectors with the quantities $x_{l,m}(1)$ and $x_{l,m}(2)$ as

$$\mathbf{e}_{l,m} = x_{l,m}(1)\mathbf{a}(1) + x_{l,m}(2)\mathbf{a}(2). \quad (1)$$

0740-3232/99/092169-08$15.00

Each element of the color vector indicates a pixel value of the corresponding channel. Denote now by $\mathbf{A} = [\mathbf{a}(1), \mathbf{a}(2)]$ the constant 2×2 mixing matrix whose column vectors are pure color vectors and by $\mathbf{x}_{l,m} = [x_{l,m}(1), x_{l,m}(2)]^t$ the quantity vector on the image coordinates (l, m). We can write the signal model in vector and matrix form as follows:

$$\mathbf{e}_{l,m} = \mathbf{A}\mathbf{x}_{l,m}. \tag{2}$$

Inoue *et al.*[10] also assumed that the elements $x_{l,m}(1)$ and $x_{l,m}(2)$ of the quantity vector are mutually independent for the image coordinates (l, m). Figure 1(a) shows the process of mixing, and Fig. 1(b) is an example of the probability density distribution of $x_{l,m}(1)$ and $x_{l,m}(2)$, which are mutually independent. Figure 1(c) shows the probability density distribution in the image, of $e_{l,m}(1)$ and $e_{l,m}(2)$ which are elements of the compound color vector $\mathbf{e}_{l,m}$. It should be noted that the observed color signals $e_{l,m}(1)$ and $e_{l,m}(2)$ are not mutually independent. In Fig. 1(c), pure color vectors $\mathbf{a}(1)$ and $\mathbf{a}(2)$ are also shown to illustrate the relationship among the parameters.

By applying ICA to the compound color vectors in the image, we extract the relative quantity and the pure color vector of each pigment without *a priori* information on the quantity and the color vector under the assumption that the quantities of pigments are mutually independent for the image coordinates. Let us define the following equation by using the separating matrix $\mathbf{H}$ and the separated vector $\mathbf{s}_{l,m}$ as shown in Fig. 1(a):

$$\mathbf{s}_{l,m} = \mathbf{H}\mathbf{e}_{l,m}, \quad \mathbf{H} = [\mathbf{h}(1), \mathbf{h}(2)],$$
$$\mathbf{s}_{l,m} = [s_{l,m}(1), s_{l,m}(2)]^t, \tag{3}$$

where $\mathbf{h}(1)$ and $\mathbf{h}(2)$ are separating vectors. By finding the appropriate separating matrix $\mathbf{H}$, we can extract the mutually independent signals $s_{l,m}(1)$ and $s_{l,m}(2)$ from the compound color vectors in the image. Many methods for finding separating matrix $\mathbf{H}$ have been proposed (for example, Refs. 11–15), such as using the learning ability of an artificial neural network[14] and optimization techniques based on the fixed-point method.[12]

The extracted independent signals $s_{l,m}(1)$ and $s_{l,m}(2)$ may correspond to $x_{l,m}(2)$ and $x_{l,m}(1)$, respectively, and it is impossible to determine the absolute quantities $x_{l,m}(1)$ and $x_{l,m}(2)$ without an additional assumption. Therefore the extracted independent vector $\mathbf{s}_{l,m}$ is given by

$$\mathbf{s}_{l,m} = \mathbf{R}\Lambda\mathbf{x}_{l,m}, \tag{4}$$

where $\mathbf{R}$ is the permutation matrix that may substitute the elements of the vectors for each other, and Λ is the diagonal matrix that relates the absolute quantities to the relative qualities. Substituting Eqs. (2) and (3) into Eq. (4) gives

$$\mathbf{H}\mathbf{A}\mathbf{x}_{l,m} = \mathbf{R}\Lambda\mathbf{x}_{l,m}. \tag{5}$$

If we take Eq. (5) in the arbitrary quantity vector, the matrix $\mathbf{HA}$ should be equal to the matrix $\mathbf{R}\Lambda$, and the mixing matrix $\mathbf{A}$ is calculated by using the inverse matrix of $\mathbf{H}$ as follows:

$$\mathbf{A} = \mathbf{H}^{-1}\mathbf{R}\Lambda. \tag{6}$$

Note that what we can obtain by ICA are relative quantities and directions of compound color vectors. In our application of color image separation and synthesis, however, the absolute values are not required.

If the number of pigments is larger than the number of channels, it is impossible to extract the independent components caused by reduction of the signals. On the other hand, if the number of pigments is smaller than the number of channels, it is possible to make the number of channels equal to the number of pigments by using principal-component analysis (PCA).[14] This technique is also used in our analysis.

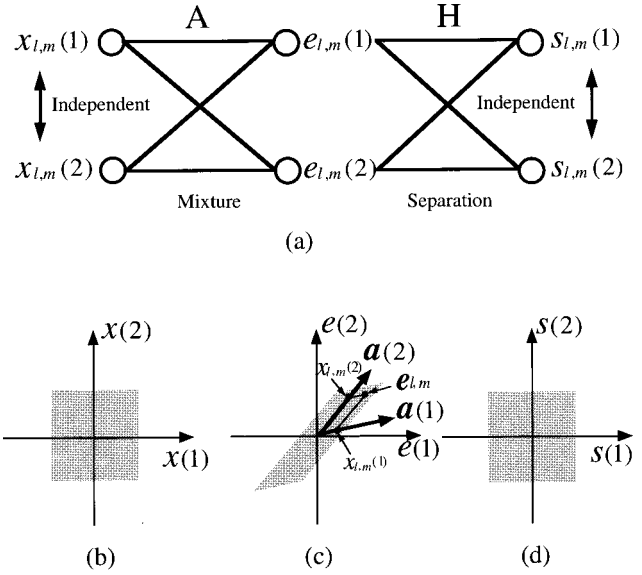

Fig. 1. Mixture and separation of independent signals: (a) flow of the signals, examples of probability density distribution of (b) $x_{l,m}(1)$ and $x_{l,m}(2)$, (c) $e_{l,m}(1)$ and $e_{l,m}(2)$, and (d) $s_{l,m}(1)$ and $s_{l,m}(2)$.

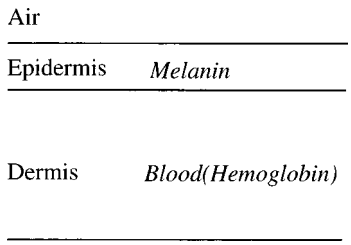

Fig. 2. Schematic model of human skin with plane-parallel epidermal and dermal layers.

3. SKIN COLOR MODEL

A schematic model of human skin is shown in Fig. 2 with plane-parallel epidermal and dermal layers. The epidermal and dermal layers are turbid media. Various pigments such as melanin, hemoglobin, bilirubin, and β-carotene are contained in the layers; in particular, melanin and hemoglobin are predominantly found in the epidermal and the dermal layer, respectively.

Figure 3(a) shows a skin color image with 64×64 pixels used for ICA. The image is extracted from the forehead of the facial image with 300×450 pixels taken by a HDTV camera (Nikon HQ1500C) with 1920×1035 pixels. The facial image is shown in Fig. 3(b), with the

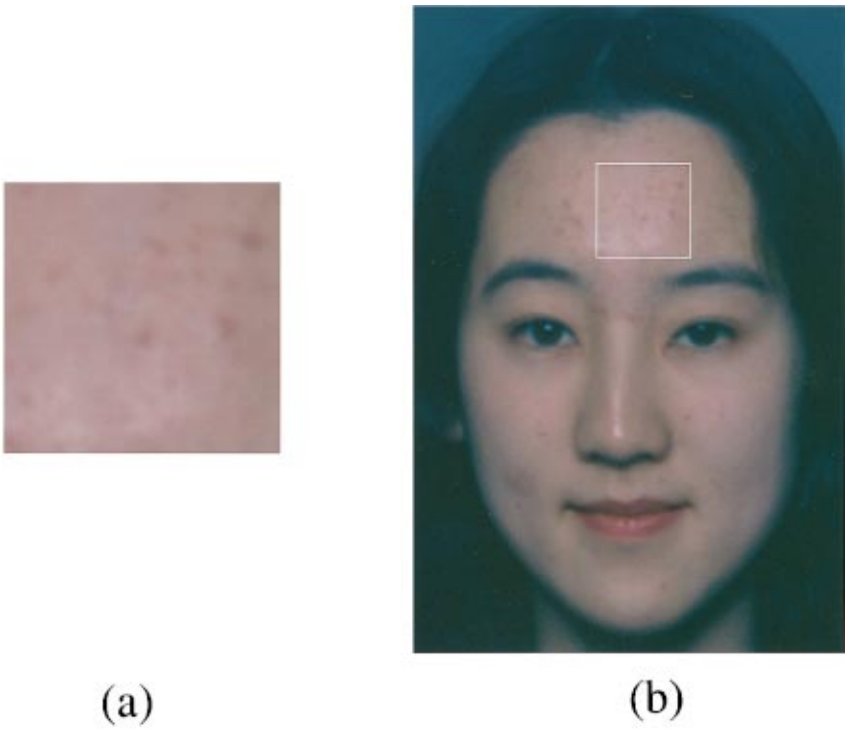

Fig. 3. Analyzed color images: (a) skin color image with 64 × 64 pixels, (b) facial image color image with 1920 × 1035 pixels. The skin color image is extracted from the forehead of the facial image. The extracted area is enclosed by a white square.

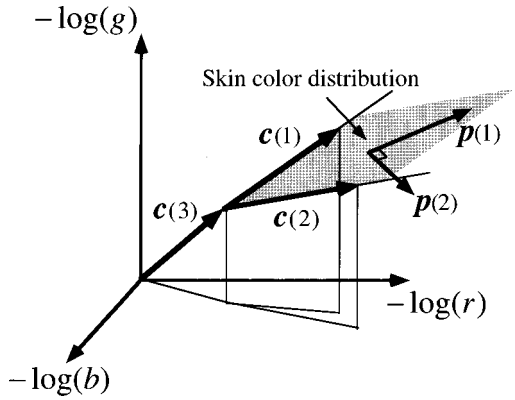

Fig. 4. Skin color model in the optical density domain of three channels.

extracted area enclosed by a white square. The subject was not wearing makeup or lipstick. Each pixel of these color images has three channels: red, green, and blue. Let $r_{l,m}$, $g_{l,m}$, $b_{l,m}$ be the pixel values in red, green, and blue channels, respectively, of the skin color image on the image coordinates (l, m).

Analyzing this skin color, we made four assumptions about skin color. First, the Lambert–Beer law, or rather the modified Lambert–Beer law,[16] holds with respect to the reflected light among the quantities and the observed color signals. Second, the spectral distribution of the skin is not abrupt in the sensitive spectral range of each channel in the imaging system. Third, the spatial variations of color in the skin are caused by two pigments: melanin and hemoglobin. Fourth, the pigment quantities are mutually independent spatially.

The first assumption ensures linearity among the observed color signals and pure color signals of the pigments in the spectral density domain. The second assumption ensures linearity in the optical density domain of three channels: $-\log(r_{l,m})$, $-\log(g_{l,m})$, and $-\log(b_{l,m})$. This is true because the signal value of each channel is obtained by integration of the spectral intensity with respect to the wavelength in the sensitive spectral range of each channel in the imaging system, and the integration can be approximated as a product of the intensity at a wavelength by a constant if the spectral distribution of the skin is approximated as flat in the sensitive spectral range. On the basis of the linearity and the third assumption, the color in the skin image is modeled in Fig. 4 in the optical density domain of three channels. It is seen that the three densities of skin color are distributed on the two-dimensional plane spanned by the pure color vectors of melanin and hemoglobin. We denote by $\mathbf{c}_{l,m}$ the color density vector on the image coordinates (l, m):

$$\mathbf{c}_{l,m} = [-\log(\mathbf{r}_{l,m}),\ -\log(g_{l,m}),\ -\log(b_{l,m})]^t, \qquad (7)$$

where $[\ \cdot\ ]^t$ represents transposition. According to the skin color model shown in Fig. 4, the color density vector of skin can be expressed by

$$\mathbf{c}_{l,m} = q_{l,m}(1)\mathbf{c}(1) + q_{l,m}(2)\mathbf{c}(2) + \mathbf{c}(3), \qquad (8)$$

where $\mathbf{c}(1)$ and $\mathbf{c}(2)$ are pure density vectors of hemoglobin and melanin (or melanin and hemoglobin); $q_{l,m}(1)$ and $q_{l,m}(2)$ are relative quantities of the pigments, respectively; and $\mathbf{c}(3)$ is the spatially stationary vector caused by other pigments and skin structure. The vectors $\mathbf{c}(1)$ and $\mathbf{c}(2)$ are normalized as $\|\mathbf{c}(1)\| = \|\mathbf{c}(2)\| = 1$, where $\|\ \cdot\ \|$ is the operation of the Euclidean norm. Equation (8) is written in vector and matrix form by using the pure color density matrix $\mathbf{C} = [\mathbf{c}(1), \mathbf{c}(2)]$ and the quantity vector $\mathbf{q}_{l,m} = [q_{l,m}(1), q_{l,m}(2)]^t$ as

$$\mathbf{c}_{l,m} = \mathbf{C}\mathbf{q}_{l,m} + \mathbf{c}(3). \tag{9}$$

It can be easily understood that ICA as described in Section 2 can be applied in the two-dimensional plane spanned by $\mathbf{c}(1)$ and $\mathbf{c}(2)$ to estimate the quantity vector $\mathbf{q}_{l,m}$ from the color density vectors $\mathbf{c}_{l,m}$. PCA is used to extract the two-dimensional plane. Figure 5 shows the relationship between the number of principal components used and the cumulative contribution ratio. The values of the three channels can be adequately described by using two principal components with an accuracy of 99.3%. Let us denote the first, second, and third principal-component vectors as $\mathbf{p}(1)$, $\mathbf{p}(2)$, and $\mathbf{p}(3)$, respectively. We note that $\mathbf{p}(1)$, $\mathbf{p}(2)$ will span the two dimensional space spanned by $\mathbf{c}(1)$ and $\mathbf{c}(2)$.

Here we define the projection matrix $\mathbf{P}\mathbf{P}^t = [\mathbf{p}(1), \mathbf{p}(2)][\mathbf{p}(1), \mathbf{p}(2)]^t$ onto the two-dimensional space spanned by $\mathbf{c}(1)$ and $\mathbf{c}(2)$. On the basis of the projection, the color density vector $\mathbf{c}_{l,m}$ can be divided into two components as follows:

$$\mathbf{c}_{l,m} = \mathbf{P}\,\mathbf{P}^t\mathbf{c}_{l,m} + (\mathbf{I} - \mathbf{P}\,\mathbf{P}^t)\mathbf{c}_{l,m}, \tag{10}$$

where matrix $\mathbf{I}$ denotes an identity matrix. The first term indicates the component in the two-dimensional subspace spanned by $\mathbf{c}(1)$ and $\mathbf{c}(2)$ or $\mathbf{p}_1$ and $\mathbf{p}_2$. The second term indicates the component in the one-dimensional subspace spanned by $\mathbf{p}_3$. Substituting Eq. (9) into Eq. (10), we show in Eq. (11) that the second term is independent of the quantities $\mathbf{q}_{l,m}$:

$$\mathbf{c}_{l,m} = \mathbf{P}\,\mathbf{P}^t\{\mathbf{C}\mathbf{q}_{l,m} + \mathbf{c}(3)\} + (\mathbf{I} - \mathbf{P}\,\mathbf{P}^t)\mathbf{c}(3). \tag{11}$$

4. SKIN COLOR IMAGE SEPARATION

The skin color model proposed in Section 3 is used to extract the unknown color density matrix $\mathbf{C}$ and the unknown relative quantity vectors $\mathbf{q}_{l,m}$. The flow chart of the extraction is shown in Fig. 6 with use of the computation in Section 3.

Let us define the score vector $\mathbf{w}_{l,m}$ in the first term of Eq. (11) as

$$\mathbf{w}_{l,m} = \mathbf{P}^t\{\mathbf{C}\mathbf{q}_{l,m} + \mathbf{c}(3)\}. \tag{12}$$

Equation (12) is rewritten as

$$\mathbf{w}_{l,m} = \mathbf{P}^t\mathbf{C}\mathbf{q}'_{l,m}, \tag{13}$$

where

$$\mathbf{q}'_{l,m} = \mathbf{q}_{l,m} + (\mathbf{P}^t\mathbf{C})^{-1}\mathbf{P}^t\mathbf{c}(3). \tag{14}$$

To make the task of ICA easier,[14] the elements in the score vector $\mathbf{w}_{l,m}$ were made zero mean by subtracting the mean vector $\bar{\mathbf{w}}$, and they were made unit variance by multiplying the inverse square root of the 2×2 diagonal matrix $\mathbf{D} = \mathrm{diag}[\lambda(1), \lambda(2)]$, where $\lambda(1)$ and $\lambda(2)$ denote the eigenvalues for the first and second principal components, respectively. The whitened vector denoted by $\mathbf{e}_{l,m}$ is written as

$$\mathbf{e}_{l,m} = \mathbf{D}^{-1/2}(\mathbf{P}^t\mathbf{C}\mathbf{q}'_{l,m} - \bar{\mathbf{w}}). \tag{15}$$

Equation (15) is rewritten as

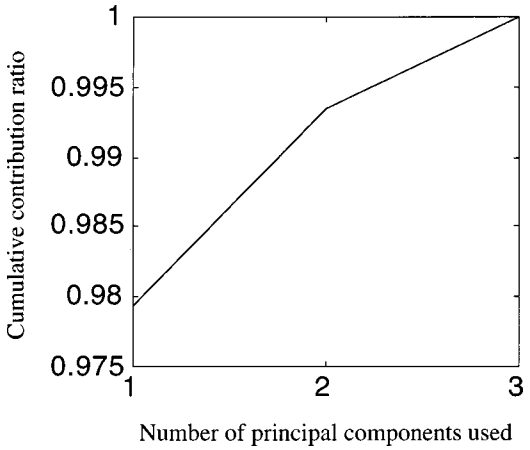

Fig. 5. Relationship between the number of principal components used and the cumulative contribution ratio in skin colors of three channels.

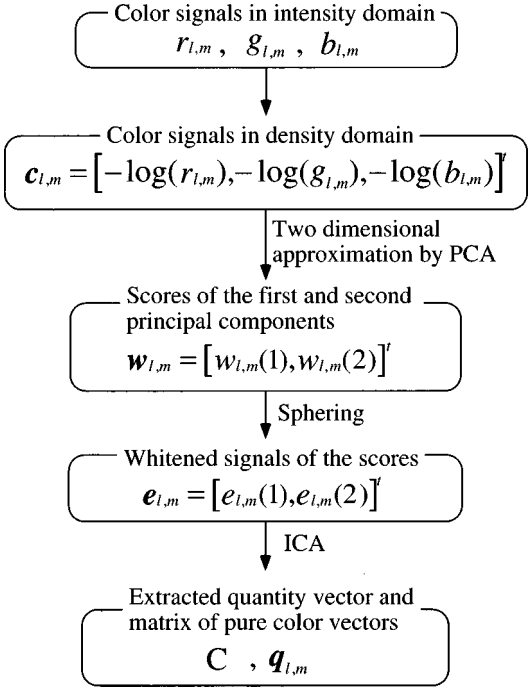

Fig. 6. Flow chart of preprocessing and ICA for a skin color image.

$$\mathbf{e}_{l,m} = \mathbf{D}^{-1/2}\mathbf{P}^t\mathbf{C}\mathbf{x}_{l,m}, \tag{16}$$

where

$$\mathbf{x}_{l,m} = \mathbf{q}'_{l,m} - (\mathbf{P}^t\mathbf{C})^{-1}\bar{\mathbf{w}}. \tag{17}$$

Here we define the $\mathbf{A} = \mathbf{D}^{-1/2}\mathbf{P}^t\mathbf{C}$, and then we get Eq. (18), which is the same as Eq. (2):

$$\mathbf{e}_{l,m} = \mathbf{A}\mathbf{x}_{l,m}. \tag{18}$$

The whitened vector $\mathbf{e}_{l,m}$ is considered the compound color vector in Eq. (2), and the vector $\mathbf{x}_{l,m}$ in Eq. (18) is considered the quantity vector in Eq. (2). The separation matrix $\mathbf{H}$ is obtained by ICA for the normalized vectors $\mathbf{e}_{l,m}$, and the mixing matrix is calculated by Eq. (6). Substituting $\mathbf{A} = \mathbf{D}^{-1/2}\mathbf{P}^t\mathbf{C}$ into Eq. (6) and solving for the color matrix $\mathbf{C}$, we calculate the estimated matrix $\tilde{\mathbf{C}}$ of pure color densities as

$$\tilde{\mathbf{C}} = (\mathbf{D}^{-1/2}\mathbf{P}^{t})^{-1}\mathbf{H}^{-1}\mathbf{R}\mathbf{\Lambda}. \tag{19}$$

The diagonal matrix $\mathbf{\Lambda}$ was chosen to normalize the matrix $\tilde{\mathbf{C}}$ as $\|\mathbf{c}(1)\| = \|\mathbf{c}(2)\| = 1$, and the permutation matrix $\mathbf{R}$ is an identity matrix in this paper.

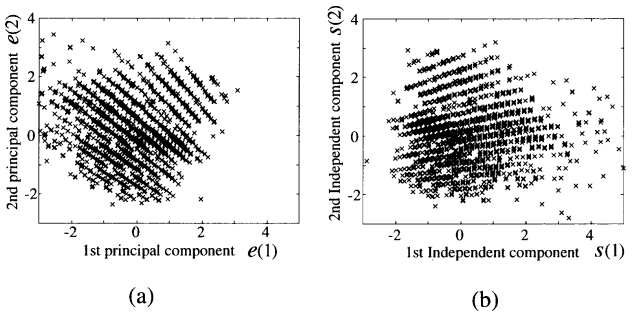

Fig. 7. Distribution of (a) observed signals $e_{l,m}(1)$ and $e_{l,m}(2)$ and (b) separated signals $s_{l,m}(1)$ and $s_{l,m}(2)$.

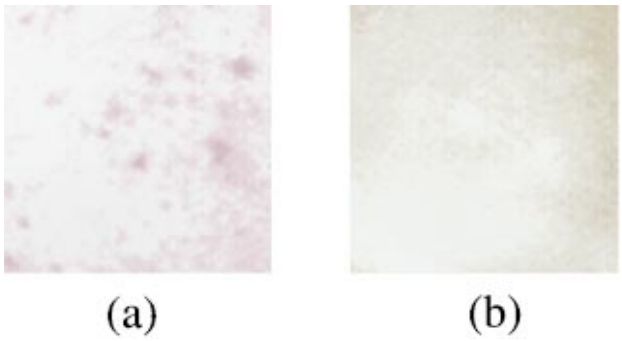

Fig. 8. Two separated independent components of the skin color image: (a) first and (b) second independent components. The synthesis parameters are set as (a) $K = \mathrm{diag}[1, 0]$ and $j = 0$, (b) $K = \mathrm{diag}[0, 1]$ and $j = 0$.

Each element of the separation matrix $\mathbf{H}$ was obtained by minimizing Burel's independence evaluation value[11] for the elements of vector $\mathbf{s}_{l,m}$. The independence evaluation value ranges from 0 to 1, and if the value is 0, the signals are mutually independent. The minimization is performed by quasi-Newton implementation with use of the MATLAB toolbox.[17] Figures 7(a) and 7(b) show the distribution of observed signals $e_{l,m}(1)$ and $e_{l,m}(2)$ and the resultant signals $s_{l,m}(1)$ and $s_{l,m}(2)$, respectively. The independence evaluation value for the observed signals and resultant signals were 0.2414 and 0.0081, respectively. We can conclude that $s_{l,m}(1)$ and $s_{l,m}(2)$ are fairly independent of each other from the independence evaluation value of 0.008[11]; therefore melanin and hemoglobin were distributed independently in the skin color image.

The quantity vector is estimated by using the estimated pure color matrix $\tilde{\mathbf{C}}$. Replacing the color matrix $\mathbf{C}$ with the estimated matrix $\tilde{\mathbf{C}}$ in Eq. (9) and solving for quantity vector $\mathbf{q}_{l,m}$, we obtain the estimated quantity vector $\tilde{\mathbf{q}}_{l,m}$:

$$\tilde{\mathbf{q}}_{l,m} = \tilde{\mathbf{C}}^{+}\mathbf{c}_{l,m} - \mathbf{b}, \tag{20}$$

where $\tilde{\mathbf{C}}^{+}$ is the Moore–Penrose generalized inverse matrix of $\tilde{\mathbf{C}}$, and $\mathbf{b}$ is defined by $\tilde{\mathbf{C}}^{+}\mathbf{c}(3)$. The vector $\mathbf{c}(3)$ is unknown, and therefore if we assume that the smallest value of each element in $\mathbf{q}_{l,m}$ in the skin image is zero, then $\mathbf{b}$ is calculated by

$$\mathbf{b} = \min_{l,m}(\tilde{\mathbf{C}}^{+}\mathbf{c}_{l,m}), \tag{21}$$

where $\min_{l,m}(\mathbf{x})$ produces the smallest element of the vector $\mathbf{x}$ in the image and gives the elements in vector form.

According to the above analysis, the color-separation-

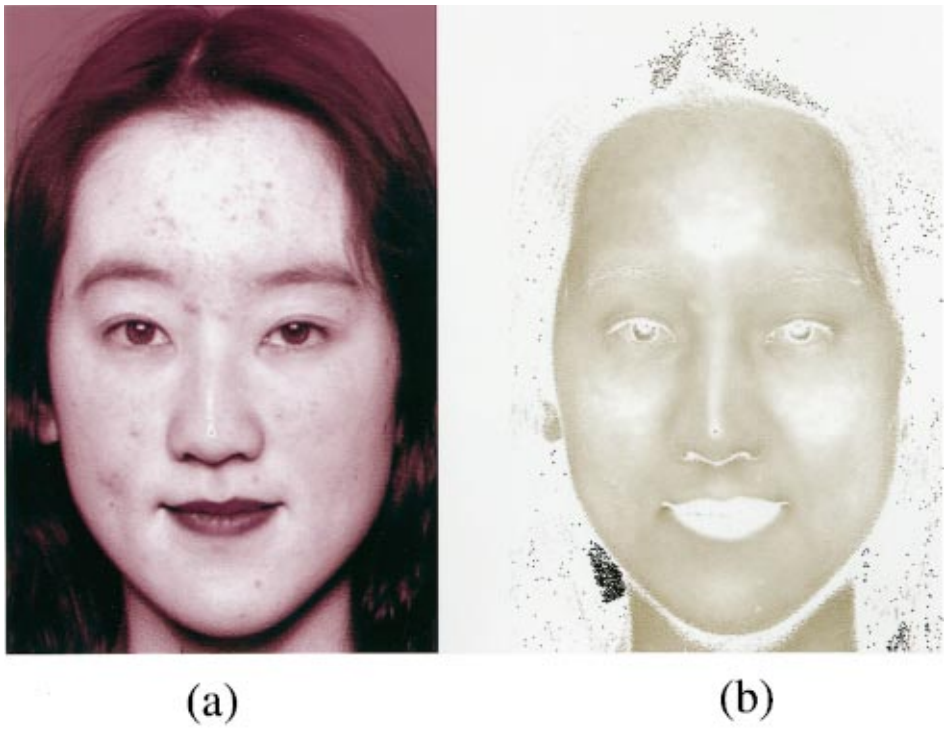

Fig. 9. Two separated images corresponding to (a) first and (b) second independent components. Synthesis parameters are set as (a) $K = \mathrm{diag}[1, 0]$ and $j = 0$, (b) $K = \mathrm{diag}[0, 1]$ and $j = 0$.

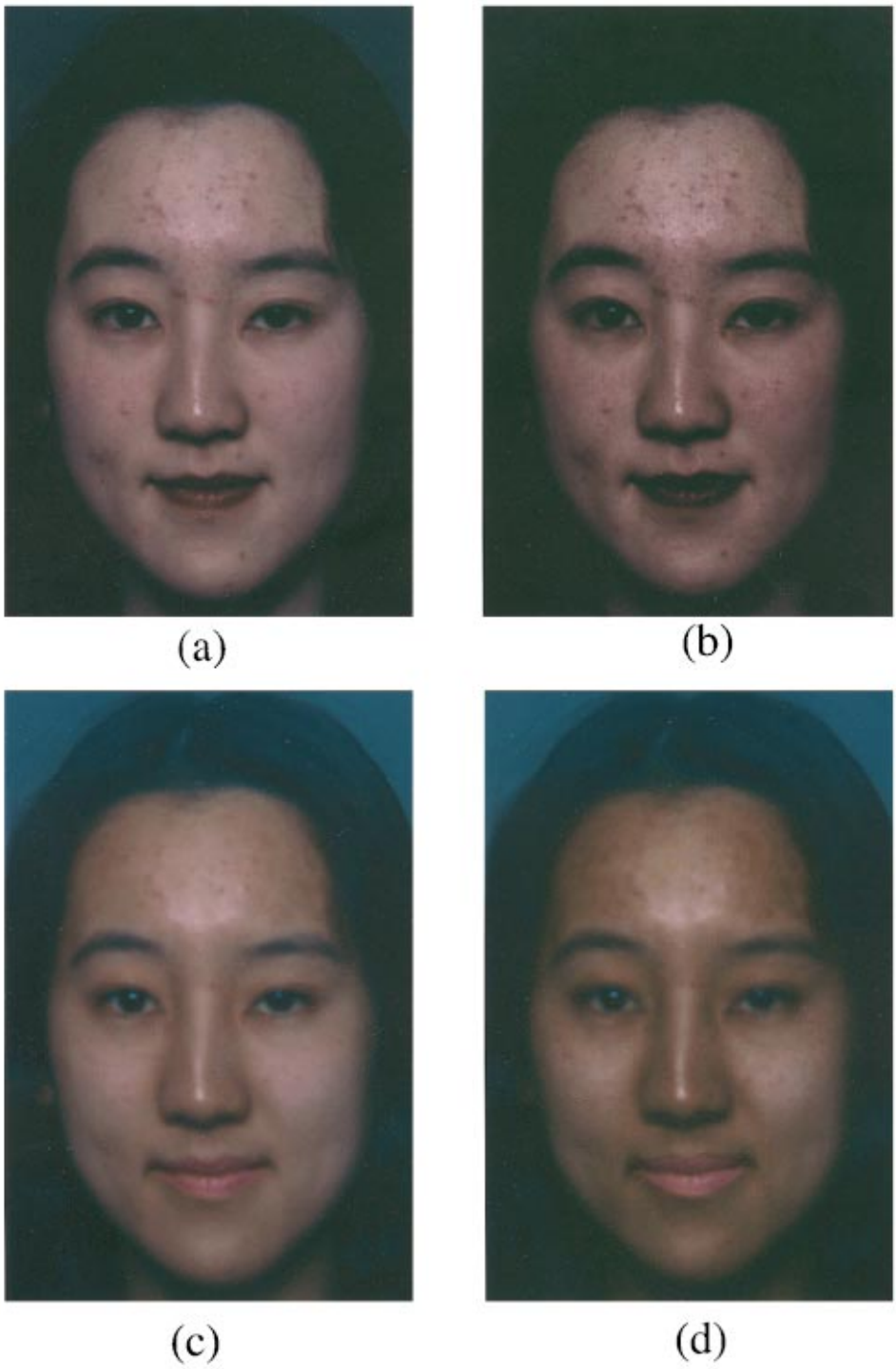

Fig. 10. Simulated images of facial color variation based on the independent component. The synthesis parameters are set as (a) K = diag[2, 1] and j = 1, (b) K = diag[3, 1] and j = 1, (c) K = diag[1, 2] and j = 1, (d) K = diag[1, 3] and j = 1.

and-synthesis equation is written as

$$\mathbf{c}'_{l,m} = \tilde{\mathbf{C}}\{K(\tilde{\mathbf{C}}^{+}\mathbf{c}_{l,m} - \mathbf{b}) + j\mathbf{b}\} + j(\mathbf{I} - \mathbf{P}\ \mathbf{P}^{t})\mathbf{c}_{l,m}, \tag{22}$$

where $\mathbf{c}'_{l,m}$ is the synthesized color, K is the diagonal matrix that changes the quantities of pigments $\mathbf{q}_{l,m}(=\tilde{\mathbf{C}}^{+}\mathbf{c}_{l,m} - \mathbf{b})$, and j is the value that changes the quantities of the stationary color vector $\mathbf{c}(3)$. We call K and j the synthesis parameters.

Figures 8(a) and 8(b) show the two separated independent components: the first and the second independent component, respectively. We set the synthesis parameters as K = diag[1, 0] and j = 0 in Fig. 8(a) and K = diag[0, 1] and j = 0 in Fig. 8(b). It is assumed that the first and the second independent components are caused by hemoglobin and melanin, respectively, since the pimples are seen in the first independent component and are not seen in the second independent component.

5. FACIAL COLOR IMAGE SEPARATION AND SYNTHESIS

The main variations of facial color are caused by the variation in the quantity of hemoglobin and melanin. It is possible to simulate facial color variation by synthesizing the two separated components with an increase or decrease of each separated quantity.

We applied the color-separation-and-synthesis equation [Eq. (22)] to the facial image shown in Fig. 3(b). The coefficients of the equation were obtained by analyzing the skin color image shown in Fig. 3(a). Figures 9(a) and 9(b) show two separated images corresponding to the first and the second independent component, respectively. We set the synthesis parameters as $K = \mathrm{diag}[1, 0]$ and $j = 0$ in Fig. 9(a) and as $K = \mathrm{diag}[0, 1]$ and $j = 0$ in Fig. 9(b). Note that there is a little melanin at the lip region in Fig. 9(b). This result agrees well with physiological knowledge. However, the region of hair is mistakenly separated into the region of hemoglobin. We considered that the skin model does not hold for hair.

Figure 10 shows simulated results of facial color variation based on the independent component. We set the synthesis parameters as $K = \mathrm{diag}[2, 1]$ and $j = 1$ in Fig. 10(a), $K = \mathrm{diag}[3, 1]$ and $j = 1$ in Fig. 10(b), $K = \mathrm{diag}[1, 2]$ and $j = 1$ in Fig. 10(c), $K = \mathrm{diag}[1, 3]$ and $j = 1$ in Fig. 10(d). If the estimated quantity at a certain point is smaller than the corresponding element of **b** in Eq. (22), the parameters are set as $K = \mathrm{diag}[1, 1]$ and $j = 1$ to hold the image quality in the regions of hair, background, and so on. It can be seen in Fig. 10(a) that the pimples are enhanced by the increase in hemoglobin, and in Fig. 10(b) the whole facial color becomes flushed, as if the subject were in a high-temperature room. It is seen in Figs. 10(c) and 10(d) that the facial colors become more brownish, as if the subject had gotten a suntan. It can also be seen that the highlights were emphasized in the synthesized image in Fig. 10. This occurred because we assumed that the smallest value of each quantity of the skin image is zero in Eq. (21). The highlights were caused by the geometry of the environmental illuminant in Fig. 10(b).

6. CONCLUSION AND DISCUSSION

The skin and the facial color images were each separated into two images by independent-component analysis (ICA) in the optical density domain of three color channels. We believe that the images correspond to distributions of melanin and hemoglobin, because the result of separation agreed well with physiological knowledge. The separated components were synthesized to simulate the various facial color images by changing the quantities of the two separated pigments.

Many assumptions were made in the analysis: (1) linearity among the quantities and the observed color signals in the optical density domain, (2) spatial color variation caused by only two pigments, (3) spatial independence of the two pigments, and (4) zero quantity at a certain point of the skin image. From the results of principal-component analysis and ICA, we can conclude that linearity, spatial color variation, and spatial independence were confirmed in our experiments. In applying this technique to various parts of the body, however, it will be necessary to consider the violation of these assumptions depending on the area of skin image, skin structure, skin condition, and so on. In addition to the above assumptions, we have assumed implicitly that pure color vectors of pigments will not change spatially. However, hemoglobin has two types of state: oxyhemoglobin (HbO_2) and deoxy-hemoglobin (Hb). The spectral absorptions are different from each other, and the ratio between HbO_2 and Hb will change spatially in a large area of skin image or in an area of skin diseases.[18] When this technique is applied to such images, ICA for skin color images should be improved by the use of an artificial neural network that is adapted to the fluctuation of the system.

The values of the three color channels are dependent on the imaging device. Therefore it was impossible to discuss the separated colors directly in this paper. The proposed techniques should be applied to a calibrated image or a spectral reflectance image.

In this paper, the quantities of pigments were simply doubled and tripled in the synthesis of facial color. Various image-processing techniques will give rich variations in facial color image, and knowledge of physiological phenomena will help to reproduce the realistic variation of facial color with these techniques.

ACKNOWLEDGMENTS

Part of this research was supported by Photographic Research Fund of the Konica Imaging Foundation.

N. Tsumura can be reached at the address on the title page or by phone or fax, 81-43-290-3262; or e-mail, tsumura@ics.tj.chiba-u.ac.jp.

REFERENCES

1. R. W. G. H. Hunt, *The Reproduction of Colour* (Fountain, London, 1995).
2. F. H. Imai, N. Tsumura, H. Haneishi, and Y. Miyake, "Principal component analysis of skin color and its application to colorimetric color reproduction on CRT display and hardcopy," J. Imaging Sci. Technol. **40**, 422–430 (1996).
3. Y. Yokoyama, N. Tsumura, H. Haneishi, Y. Miyake, J. Hayashi, and M. Saito, "A new color management system based on human perception and its application to recording and reproduction of art printing," in *Proceedings of IS&T/SID 5th Color Imaging Conference, Color Science, Systems and Applications* (Society for Imaging Science & Technology, Springfield, Va., 1997), pp. 169–172.
4. P. Hanarahan and W. Krueger, "Reflection from layered surfaces due to subsurface scattering," *Proceedings of SIGGRAPH 93* (Association for Computing Machinery, New York, 1993), pp. 165–174.
5. M. Yamaguchi, R. Iwama, Y. Ohya, T. Obi, N. Ohyama, and Y. Komiya, "Natural color reproduction in the television system for telemedicine," in *Medical Imaging 1997: Image Display*, Y. Kim, ed., Proc. SPIE **3031**, 482–489 (1997).
6. M. J. C. van Gemert, S. L. Jacques, H. J. C. M. Sternborg, and W. M. Star, "Skin Optics," IEEE Trans. Biomed. Eng. **36**, 1146–1154 (1989).
7. R. R. Anderson and J. A. Parrish, "The optics in human skin," Invest. Dermatol. **77**, 13–19 (1981).
8. E. A. Edwards and S. Q. Duntley, "The pigments and color of living human skin," Am. J. Anat. **65**, 1–33 (1939).
9. J. Karhunen, A. Hyvarinen, R. Vigário, J. Hurri, and E.

Oja, "Applications of neural blind separation to signal and image processing," in *Proceedings of IEEE International Conference on Acoustics, Speech, and Signal Processing* (IEEE Computer Society Press, Los Alamitos, Calif., 1997), Vol. 1, pp. 131–134.
10. T. Inoue, Y. Fujii, K. Itoh, and Y. Ichioka, "Block blind separation of independent spectra in hyperspectral-images," in *1996 International Topical Meeting on Optical Computing: Technical Digest* (Japan Society for Applied Physics, Tokyo, 1996), Vol. 1, pp. 40–41.
11. G. Burel, "Blind separation of sources: a nonlinear neural algorithm," Neural Networks **5**, 937–947 (1992).
12. A. Hyvärinen and E. Oja, "A fast fixed-point algorithm for independent component analysis," Neural Comput. **9**, 1483–1492 (1997).
13. C. Jutten and J. Hearult, "Blind separation of sources, part I: an adaptive algorithm based on neuromimetic architecture," Signal Process. **24**, 1–10 (1991).
14. J. Karhunen, E. Oja, L. Wang, R. Vigário, and J. Joutensalo, "A class of neural networks for independent component analysis," IEEE Trans. Neural Netw. **8**, 486–504 (1997).
15. H. H. Yang and S. Amari, "Adaptive online learning algorithms for blind separation: maximum entropy and minimum mutual information," Neural Comput. **9**, 1457–1482 (1997).
16. M. Hiraoka, M. Firbank, M. Essenpreis, M. Cope, S. R. Arridge, P. v. d. Zee, and D. T. Delpy, "A Monte Carlo investigation of optical pathlength in inhomogeneous tissue and its application to near-infrared spectroscopy," Phys. Med. Biol. **38**, 1859–1876 (1993).
17. A. Garce, *MATLAB Optimization Toolbox User's Guide* (The MathWorks, Boston, Mass., 1992).
18. P. J. Dwyer, R. R. Anderson, and C. A. DiMarzio, "Mapping blood oxygen saturation using a multi-spectral imaging system," in *Biomedical Sensing, Imaging, and Tracking Technolgies II*, T. Vo-Dinh, R. A. Lieberman, and G. G. Vurek, eds., Proc. SPIE **2976**, 270–280 (1997).